

Lattice vibrations in crystalline C_{70}

P. H. M. van Loosdrecht, M. A. Verheijen, H. Meekes, P. J. M. van Bentum,* and G. Meijer
Research Institute of Materials, University of Nijmegen, Toernooiveld, 6525 ED Nijmegen, The Netherlands
 (Received 27 August 1992)

Raman spectroscopy in single-crystalline C_{70} at low temperatures reveals a large number of Raman-active intramolecular modes, consistent with the selection rules and in agreement with theoretical predictions. Librational and vibrational lattice modes are observed in the low-frequency region of the spectrum, consistent with the selection rules for monoclinic $P112_1/m-C_{70}$. We discuss the lattice modes in terms of a simplified model of the crystal potential. Near 280 K we observe a phase transition, which is assigned to the order-disorder transition for the rotational motion around the long molecular axis.

The discovery¹ of the carbon cage fullerenes and in particular the development of an efficient method² to produce macroscopic quantities of this new form of carbon sparked an intense effort to reveal and understand the physical and chemical properties of these exciting new materials, both in the molecular and in the condensed state.³ The fullerenes provide a unique form of a molecular solid where the intermolecular binding is rather weak and the nearly spherical shape of the molecules provides a large degree of rotational freedom. While the structure, electronic properties, and crystal dynamics of the more symmetrical prototype C_{60} are reasonably understood, little is known about the crystal potential and the dynamics of solid C_{70} . Only recently has one succeeded in growing C_{70} single crystals of sufficient size and quality to allow a careful crystallographic and optical investigation.

The room-temperature crystal structure of solid C_{70} was originally found to be highly defected fcc.⁴ Verheijen *et al.*⁵ showed this phase to be a true defect phase, and showed the actual room-temperature structure to be a deformed-hexagonal-close-packed (dhcp) structure, with rotational freedom around the long molecular axis. The molecular anisotropy of C_{70} gives rise to two rotational ordering transitions in the solid state.⁴ Near 270 K the disordered rotations around the long molecular axis freeze out resulting in a monoclinic ($P112_1/m$, $Z=4$) crystal structure. Slightly above room temperature (around 335 K) the rotations around the short molecular axes also become disordered yielding an ideal hcp phase. At still higher temperature, an irreversible phase transition to a perfect fcc crystal structure occurs.⁵

In this paper we present Raman experiments on both the intramolecular (internal) and intermolecular (lattice) modes of single-crystalline C_{70} at low temperature. The results are consistent with the proposed monoclinic superstructure of crystalline C_{70} at low temperatures and with the proposed approximation of the crystal potential.⁵

The C_{70} crystals used in this work are grown from the vapor phase by sublimation of high-purity C_{70} .⁵ Mass spectroscopy of the chromatographically purified starting material as well as of the obtained crystals showed no

traces of C_{60} or residual solvents (purity > 99.5%). No sign of C_{60} is observed in the Raman spectra. X-ray and electron-diffraction experiments and high-resolution electron microscopy showed that crystals with a hcp morphology are indeed also microscopically hcp ($P6_3/mmc$, $Z=2$). For the Raman experiments crystals with the hcp growth habit are chosen. To avoid surface contamination, the crystals are cut in air and immediately thereafter mounted in an optical flow cryostat (stabilization ± 0.2 K, absolute error ± 2 K) which is subsequently evacuated to $P \approx 10^{-6}$ mbar.

Unpolarized Raman spectra have been recorded with a DILOR XY multichannel Raman spectrometer using either an Ar^+ ion laser (514 nm) or a Ti:sapphire laser (771 nm) as the excitation source. The small penetration depth ($< 1 \mu\text{m}$) in crystalline C_{70} at 514 nm makes spectra recorded using this wavelength sensitive to surface effects. The much larger penetration depth ($>> 10 \mu\text{m}$) at 771 nm make this excitation wavelength better suited to probe the solid-state properties of C_{70} . The irradiance is kept below $5\text{W}/\text{cm}^2$ in order to minimize optically induced changes in the structural and electronic properties of C_{70} .⁶

Figure 1 shows two unpolarized Raman spectra of solid C_{70} at $T=23$ K recorded using 771-nm (upper curve) and 514-nm (lower curve) excitation. The spectra are recorded with a spectral slit width of 1.5 cm^{-1} and 3.5 cm^{-1} for 771-nm and 514-nm excitation, respectively. The spectral intensity is corrected for the system response (to within 20%). The increase in background signal above 1000 cm^{-1} in the 771-nm spectrum is caused by weak luminescence originating from electronically excited C_{70} . The position of the phonon modes is independent of the excitation wavelength although the relative intensities vary strongly due to electronic resonance effects and differences in penetration depth. Similar effects have been observed in C_{60} .^{7,8}

The spectrum of C_{70} is rather complex due to the relatively low D_{5h} symmetry of the molecule. The molecular selection rules predict 53 Raman-active modes which are classified as $12A'_1 + 22E'_2 + 19E'_1$. One can expect Davydov splittings and activation of molecular inactive modes to occur in solid C_{70} , as is the case for C_{60} .^{9,10} The

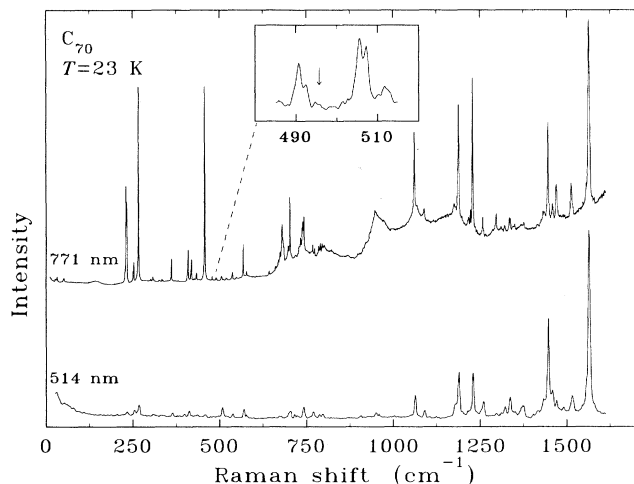


FIG. 1. Unpolarized Raman spectrum of crystalline C_{70} at $T=23$ K using 771-nm (upper curve) and 514-nm (lower curve) excitation. The large number of observed modes reflects the relatively low D_{5h} symmetry of C_{70} . The inset shows the absence of the 496-cm^{-1} A_g breathing mode of C_{60} (indicated by the arrow) in the C_{70} spectra.

selection rules in $P112_1/m-C_{70}$ ($Z=4$, site symmetry C_s) predict 408 Raman-active modes, including activation of all 122 molecular modes. The 74 clearest modes observed in the 771-nm spectrum, and given in Table I, are assumed to correspond to molecular modes. The C_{70} spectra of Fig. 1 show a peak at 1471 cm^{-1} , the position of the A_g pentagonal pinch model of C_{60} .¹¹ The absence of the C_{60} A_g breathing mode in the spectra (see inset Fig. 1) indicates that this mode originates from C_{70} , rather than from the presence of C_{60} impurities. The spectra presented here are consistent with the data reported by Bethune *et al.*¹¹ As expected from the selection rules, all reported ir-active modes are observed in the Raman spectrum as well. A fair agreement is found with the theoret-

ical data of Bakowies and Thiel,¹² provided their data are scaled with a factor 0.9 as suggested by them. In particular, the predicted absence of modes in the $800\text{--}1000\text{-cm}^{-1}$ region is experimentally confirmed. Based on the intensities, the underlined modes in Table I are tentatively assigned to the nondegenerate A'_1 molecular modes of C_{70} . The rms deviation between these modes and the theoretical A'_1 prediction is 31 cm^{-1} .

Although solid-state effects are evident in the internal mode region as discussed above, their clearest manifestation is found in the lattice mode region ($0\text{--}100\text{ cm}^{-1}$). Figure 2(a) shows two examples (circles) of the low-frequency part of the unpolarized 771-nm Raman spectrum recorded at $T=23$ K on two different crystals from the same growth batch. Based on morphological considerations we assume that the surface measured in the upper spectrum is the $\{001\}$ face, while for the lower spectrum it is the $\{101\}$ face. Several Raman-active librational and vibrational phonon modes are observed. Although the relative intensities for the two crystal faces are different, the various modes are found at the same frequencies. It should be noted that the spectra do not depend on the spot position on a certain crystal face, and that only a weak polarization dependence is found.

The solid curves through the data points in both spectra are fits of Lorentzian lines centered at the frequencies indicated in the figure with a typical full width at half maximum (FWHM) of $\sim 2\text{ cm}^{-1}$, superimposed on a Gaussian background. The latter is due to insufficient suppression of the Rayleigh peak when using the multichannel detector. In single-channel measurements the Rayleigh contribution is absent for $\omega > 3\text{ cm}^{-1}$ and no features are found between 3 and 10 cm^{-1} .

The observation of the 11 lattice modes [indicated in Fig. 2(a)] is in agreement with the monoclinic superstructure at low temperatures. The phonon modes for $P112_1/m-C_{70}$ are given by $\Gamma_{\text{ext}}^v = 4A_g^v + 2B_g^v + 2B_u^v + A_u^v$ and $\Gamma_{\text{ext}}^l = 2A_g^l + 4B_{g_l}^l + 2B_u^l + 4A_u^l$, where the superscripts denote vibrational (v) and librational (l) modes. Only the 12 gerade lattice modes are Raman active, and

TABLE I. Peak frequencies (in cm^{-1}) in the unpolarized 771-nm Raman spectrum of crystalline C_{70} at $T=23$ K. The relative intensities and full widths at half maximum intensity (in cm^{-1}) for each peak are given next to the frequency values. The underlined frequencies are assigned to the A'_1 molecular modes of C_{70} . Only the clearest peaks and shoulders are given.

228	4.0	1.3	434	3.6	1.6	677	4.7	1.8	795	4.2	2.8	1311	1.6	2.7
231	44.4	1.4	<u>458</u>	97.8	1.4	680	16.7	2.2	800	1.4	3.0	1322	2.8	4.4
233	35.6	1.4	479	2.0	1.4	683	8.6	34.0	948	2.0	2.0	1335	6.4	2.4
252	4.4	3.0	491	1.3	1.6	685	5.0	1.8	<u>1061</u>	35.1	2.1	1338	5.3	1.9
253	8.3	1.3	506	1.9	1.8	697	3.0	1.3	1069	1.6	2.0	1351	1.4	2.5
<u>267</u>	100.0	1.4	507	1.4	1.2	<u>703</u>	30.1	1.2	1089	5.1	5.3	1377	2.0	3.5
303	1.1	2.0	520	1.0	2.4	729	3.4	2.9	1176	5.1	5.8	1432	2.5	2.0
309	2.1	2.6	523	0.6	1.5	733	6.5	2.5	1187	12.9	3.0	<u>1447</u>	48.5	2.7
335	1.1	1.3	537	3.5	2.2	738	5.3	2.8	<u>1189</u>	52.1	2.4	1459	8.9	4.1
338	0.7	1.0	<u>569</u>	16.4	1.3	740	11.9	3.3	1217	4.0	3.1	1471	19.0	4.8
<u>362</u>	11.2	1.4	578	2.4	1.8	<u>743</u>	14.8	1.7	1223	7.1	1.6	<u>1514</u>	16.5	5.0
408	3.2	1.9	643	1.9	1.6	768	4.2	1.6	<u>1229</u>	73.3	2.2	1557	4.5	1.6
410	14.6	1.4	661	2.1	1.9	774	3.3	1.3	1258	9.0	2.2	<u>1565</u>	93.1	4.4
418	4.0	1.4	670	3.1	2.6	785	4.0	2.8	1261	1.7	1.5	1568	15.3	1.7
420	10.1	1.3	674	5.8	2.9	790	4.9	2.1	1297	8.4	3.0			

two of the A_g^v modes are expected to be (nearly) degenerate.

In Fig. 2(b) the low-frequency part of the spectrum is shown for temperatures close to the rotational ordering transition. It is clear that the various modes broaden considerably when approaching the phase transition. At room temperature only a weak, broad feature around 23 cm^{-1} survives. In the dhcp phase (above 335 K) no lattice modes are observed. In Fig. 3 we have plotted the peak frequencies of the various modes as a function of temperature. From the abrupt change near 280 K it is clear that the selection rules for the vibrational and librational lattice modes change dramatically when the rotational motion around the long axis lifts the nonequivalence of neighboring molecules. Verheijen *et al.*⁵ reported the $P112_1/m-C_{70} \rightarrow \text{dhcp}-C_{70}$ phase transition to occur around 270 K . In the dhcp phase

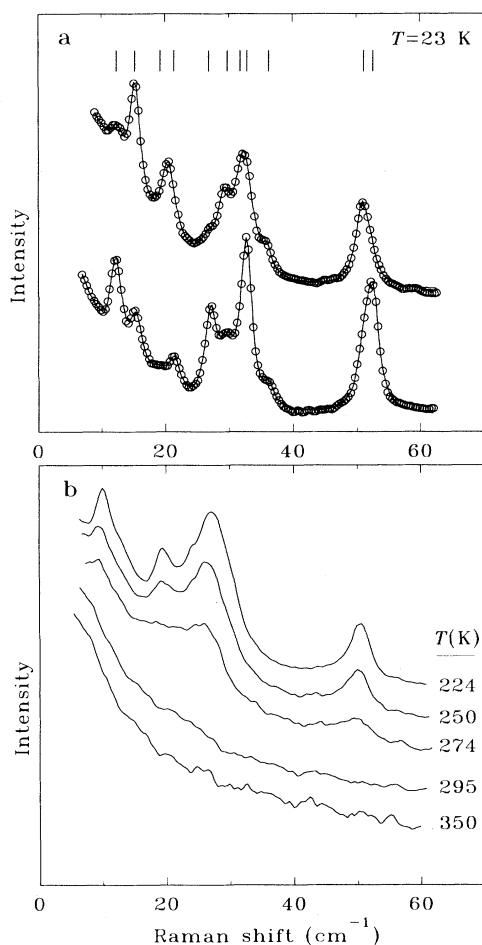


FIG. 2. (a) Low-frequency part of the unpolarized Raman spectrum ($T=23\text{ K}$) recorded using 771-nm excitation showing the lattice modes of crystalline C_{70} for two different crystals (circles). Upper curve: $\{001\}$ face; lower curve: $\{101\}$ face. The solid lines are fits of Lorentzians to the data, whose resonance frequencies are $12, 15, 19, 21, 27, 30, 32, 33, 36, 51,$ and 53 cm^{-1} , as is indicated by the markers. (b) Unpolarized 771-nm lattice mode spectrum of crystalline C_{70} near the rotational phase transition for $T=224, 250, 274, 295,$ and 350 K .

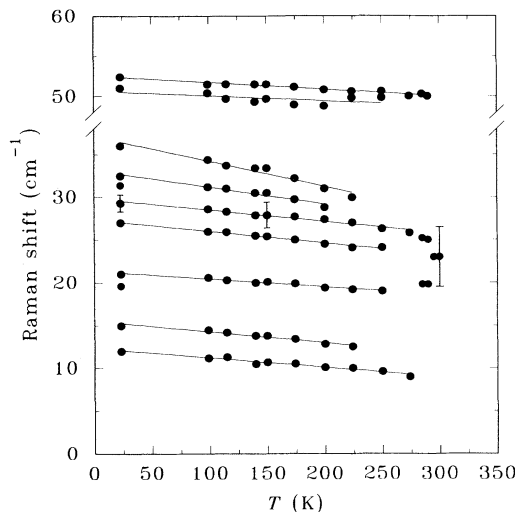


FIG. 3. Temperature dependence of the peak frequencies of the observed lattice modes. The solid lines are a guide to the eye. Most prominent is the disappearance of most of the modes above 280 K , indicating the rotational order-disorder phase transition.

($\Gamma = A_{2g}^l + B_{2g}^v + E_{1g}^l + E_{2g}^v + B_{2u}^l + E_{2u}^l$) one expects only two doubly degenerate modes; a vibrational mode with motions in the x - y plane, and a librational mode with rotations around the short molecular axes. Both modes will have approximately the same frequency. Hence, the 23-cm^{-1} feature could result from activity of both the E_g^v and E_g^l modes of the dhcp phase. The low intensity and broadening are not unexpected in view of the rotational disorder. In addition to the changes above 280 K , a weak change in the temperature dependence of some of the modes is observed near 150 K .

A reasonable estimate of the vibrational frequencies is obtained by calculating the eigenvalues of the dynamical matrix of a simple force-constant model for $P112_1/m-C_{70}$, including nearest- and next-nearest-neighbor interactions only. A suitable theoretical model for the lattice energy in the dhcp phase, which agrees well with experimental structure results,⁵ is obtained by considering a Lennard-Jones type of interaction [$\sigma=3.24\text{ \AA}$ and $\epsilon=3.68\text{ meV}$ (Ref. 5)] between rings of carbon atoms in a C_{70} molecule rotating around its long molecular axis. The unit-cell dimensions found by minimizing the lattice energy in the dhcp phase are $a=b=9.9\text{ \AA}$, and $c=18.4\text{ \AA}$. The interaction potential thus found for the dhcp phase is used as an approximation for the potential in the monoclinic phase. Additional electrostatic interactions, which are probably needed to correctly describe the low-temperature structure, are neglected.¹³ The force constants needed in the dynamical model are the one between two nearest neighbors in the $z=c/4$ plane for in plane vibrations (γ), and those between the next-nearest neighbors in the $z=c/4$ and $z=3c/4$ planes for in- and out-of-plane vibrations (α_x and α_z , respectively). The force constants for the dynamical model are determined by calculating the second derivative of the crystal

potential with respect to the vibrational displacements to give $\alpha_x = 8.4 \text{ kg s}^{-2}$, $\alpha_z = 13.8 \text{ kg s}^{-2}$, $\gamma = 20.4 \text{ kg s}^{-2}$. From the eigenvalues of the dynamical matrix we expect four A_g^v modes with polarizabilities in the ab plane at 29, 32 (doubly degenerate), and 56 cm^{-1} , respectively, and two B_g^v modes polarized along the c axis at 33 and 58 cm^{-1} . We indeed find experimentally two groups of modes around 32 and 52 cm^{-1} . Although the agreement is rather striking, it may be somewhat fortuitous in view of the various approximations and the neglect of electrostatic interactions.

A prediction of the librational frequencies cannot easily be given with sufficient accuracy within this simple model. Cheng and Klein¹⁴ performed a molecular-dynamics simulation, using a different Lennard-Jones type of interaction potential ($\sigma = 3.4 \text{ \AA}$ and $\epsilon = 2.41 \text{ meV}$). At low temperatures they find a triclinic crystal structure with a librational density of states characterized by six modes in the $5\text{--}15\text{-cm}^{-1}$ region. The absolute value of these theoretical predictions is about a factor of 2 lower than that found experimentally. This may be partly due to the specific choice of the potential parameters and partly by the neglect of electrostatic interactions. Tentatively one could assign the two lowest-frequency modes to librations involving rotations around the long

molecular axis, and a group of four modes in the $18\text{--}35\text{-cm}^{-1}$ range to those involving rotations about the short axes. A definitive assignment of the various vibrational and librational modes has to await a more detailed calculation of the molecular dynamics.

In summary, the low-temperature Raman spectrum of high-purity single-crystalline C_{70} has been presented revealing a large number of Raman-active internal modes, consistent with the selection rules. A reasonable agreement is found with the theoretically predicted frequencies.

The low-frequency Raman spectrum reveals 11 lattice modes with only a weak polarization dependence, consistent with the selection rules for a monoclinic superstructure at low temperature. A simple force-constant model for the vibrational lattice modes is found to be in good agreement with the observed spectrum. The frequencies of the librational modes are found to be nearly twice the value of recent theoretical predictions. Combining the data presented here with a full molecular-dynamics simulation can lead to a better understanding of the crystal potential, and thus of the crystal structure and phase transitions in C_{70} . The expected $P112_1/m-C_{70} \rightarrow \text{dhcp-}C_{70}$ phase transition is observed by the disappearance of most of the lattice modes above $T = 280 \text{ K}$.

*Also at IBM Thomas J. Watson Research Center, Yorktown Heights, NY 10598.

¹H. W. Kroto *et al.*, *Nature (London)* **318**, 16 (1985).

²W. Krätschmer *et al.*, *Nature (London)* **347**, 354 (1990).

³R. E. Smally (unpublished).

⁴G. B. M. Vaughan *et al.*, *Science* **254**, 1350 (1991).

⁵M. A. Verheijen *et al.*, *Chem. Phys.* **166**, 287 (1992).

⁶P. H. M. van Loosdrecht, P. J. M. van Bentum, and G. Meijer (unpublished).

⁷M. Matus, H. Kuzmany, and W. Krätschmer, *Solid State Commun.* **80**, 839 (1991).

⁸P. H. M. van Loosdrecht *et al.*, *Chem. Phys. Lett.* **198**, 587 (1992).

⁹P. H. M. van Loosdrecht, P. J. M. van Bentum, and G. Meijer, *Phys. Rev. Lett.* **68**, 1176 (1992).

¹⁰L. R. Narasimhan *et al.*, *Phys. Rev. B* **46**, 2591 (1992).

¹¹D. S. Bethune *et al.*, *Chem. Phys. Lett.* **179**, 181 (1991).

¹²D. Bakowies and W. Thiel, *Chem. Phys.* **151**, 309 (1991).

¹³M. Sprik, A. Cheng, and M. L. Klein, *J. Phys. Chem.* **96**, 2027 (1992).

¹⁴A. Cheng and M. L. Klein, *Phys. Rev. B* **46**, 4958 (1992).